The kinetic study of excited singlet oxygen atom O(1 D) reactions with acetylene

Chao Yan[*1], *Chu C. Teng*[2], *Timothy Chen*[1], *Hongtao Zhong*[1], *Aric Rousso*[1], *Gerard Wysocki*[2], *Yiguang Ju*[1]

[1]Department of Mechanical and Aerospace Engineering, Princeton University, Princeton, NJ 08544, USA

[2]Department of Electrical Engineering, Princeton University, Princeton, NJ 08544, USA

[*]Corresponding Author

Dr. Chao Yan, Associate Research Scholar

Department of Mechanical Engineering, Princeton University

D329B Engineering Quadrangle Olden Street, Princeton NJ, 08544, USA

Email Address: Chaoy@princeton.edu

Understanding the multi-channel dynamics of $O(^1D)$ reactions with unsaturated hydrocarbon molecules in low temperature reaction kinetics is critically important in stratospheric chemistry, plasma chemistry, and plasma assisted fuel reforming, materials synthesis, and combustion. A photolysis flow reactor coupled with highly selective mid-infrared Faraday Rotation Spectroscopy (FRS) and direct UV-IR absorption spectroscopy (DAS) techniques was developed for the first time to study the multi-channel dynamics of excited singlet oxygen atom $O(^1D)$ reactions with C_2H_2 and the kinetics of subsequent reactions. Time-resolved species concentrations of $O(^1D)$, OH, HO_2 and H_2O were obtained and used to develop a validated kinetic model of $O(^1D)$ reactions with C_2H_2. The branching ratios of $O(^1D)$ reaction with C_2H_2 and subsequent HO_2 kinetics were also quantified. It is found that, contrary to $O(^1D)$ reactions with saturated alkanes, OH formation via direct H abstraction by $O(^1D)$ is negligible. The results revealed that two chain-branching and propagation reactions via direct $O(^1D)$ insertion are the major pathways for radical production. Moreover, a new reaction pathway for low temperature HO_2 production via $C_2H_2OH + O_2$ is identified and its reaction rate is determined. The present study clearly demonstrated the advantage of radical detection and kinetic studies using FRS in the effective suppression of absorption interference from non-paramagnetic hydrocarbons.

TOC GRAPHICS

KEYWORDS: Singlet oxygen atom; Atmospheric Kinetics; Photolysis Herriott cell; Faraday rotation spectroscopy; Balanced Detection; Plasma assisted combustion.

1. Introduction

The chemical behavior of electronically excited singlet oxygen atom, $O(^1D)$, is of considerable interest and remains experimentally attractive throughout the past few decades due to its substantial roles in establishing chemical composition of atmospheric chemistry, plasma fuel reforming, plasma assisted materials synthesis and combustion.[1-2] Numerous studies[3-5] have shown that $O(^1D)$ atoms contribute significantly to enhance ignition, reform fuel, and reduce emissions. In particular, $O(^1D)$ plays an important role in accelerating low temperature chain branching, leading to the formation of cool flames and warm flames.[6-7] Moreover, $O(^1D)$ also contributes to the oxidation of leaked fuels and unburned hydrocarbons as well as the O_3 cycle in the atmosphere.[8-9] As such, understanding the multi-channel dynamics of the $O(^1D)$ reaction with fuel molecules and the low temperature reaction kinetics is critical. However, $O(^1D)$ reactions with fuels are complicated by its multi-channel behavior due to direct oxygen atom insertion process.

Early studies[10-15] of the reaction between $O(^1D)$ with saturated hydrocarbons have been conducted to understand the role of $O(^1D)$ initiated chain-branching reactions. In reaction dynamic studies, the products and branching ratios of the reaction channels are quite different because of the competition among different channels after oxygen atom insertion. In these reactions, the dominant reaction mechanism is the oxygen atom insertion into C-H bond, while direct H abstraction in the OH formation channel and oxygen atom insertion into the C-C bond are also important in some cases for larger hydrocarbons.

Unfortunately, for even a simple unsaturated hydrocarbon such as C_2H_2, the multi-channel dynamics of its reaction with $O(^1D)$ and the kinetics of subsequent reactions are not well understood. Limited relevant studies are available: Shaun A. C. experimentally studied the reaction between $O(^1D)$ and C_2H_2 and reported the rate constant which was adopted in the current model.[16]

Yvan and Patrick theoretically studied the primary addition reactions of $O(^1D)$ with C_2H_2 without considering secondary bond cleavage reactions, and the secondary products were estimated to be H, C_2OH, OH, C_2H and HCCO.[17] Based on this estimation, four potential reaction channels are considered in the current reaction mechanism:

$$O(^1D) + C_2H_2 \rightarrow HCCOH \qquad R_{1a} \qquad (1)$$

$$O(^1D) + C_2H_2 \rightarrow HCCO + H \qquad R_{1b} \qquad (2)$$

$$O(^1D) + C_2H_2 \rightarrow CH_2 + CO \qquad R_{1c} \qquad (3)$$

$$O(^1D) + C_2H_2 \rightarrow C_2H + OH \qquad R_{1d} \qquad (4)$$

In addition, the radicals formed during these secondary chain-branching reactions initialize further chain-propagation and chain-branching reactions. Formation of radicals (i.e. OH and HO_2) due to the subsequent hydrocarbon oxidation reactions are therefore extremely important. Understanding the multi-channel dynamics and subsequent reaction kinetics of $O(^1D)$ with C_2H_2 is critical to understanding $O(^1D)$ kinetics with larger unsaturated fuels and unburned hydrocarbons typically containing alkenes and aldehydes.

Time-resolved diagnostics of radical species is crucial in kinetic studies due to the short-lived nature of free radicals. Many spectroscopic techniques have been adopted for radical species detection, the most notable examples include ultraviolet (UV) and mid-infrared (IR) tunable laser absorption spectroscopy (TDLAS), laser-induced fluorescent spectroscopy (LIF), and cavity ring-down spectroscopy (CRDS).[18-24] For LIF, HO_2 is measured indirectly through chemical conversion to OH, and in many cases uncontrolled reactions involving the peroxy radicals

introduce significant experimental uncertainty. Moreover, the sensitivity is limited by fluorescence quenching and uncertainty in OH detection.[21-22]

For CRDS, the acquisition interval is limited by the time required to have sufficient intensity build-up in the cavity and radical quenching on the sampling nozzle.[23] TDLAS in principle can provide much better time resolution; however, sensitive measurement of radicals (e.g. RO_2 and HO_2) in both CRDS and TDLAS is challenging due to spectral contaminations from H_2O_2, H_2O, and other hydrocarbons in the mid-IR and UV regions[25-26]. Typically, the efficacy of TDLAS depends on identifying a spectral region free from unwanted absorption features, which becomes challenging in higher pressure experiments, and is compounded when using larger fuels with broadband spectral features.[18, 23, 27]

To this end, Brumfield et al. first applied Faraday rotation spectroscopy (FRS) for HO_2 detection at the exit of a laminar flow reactor[27]. A modulated magnetic field was used to improve the detection limit and remove spectral interference. However, no time dependent measurements were attempted due to the slow field modulation.

In this work, we aim to study the multi-channel dynamics of excited singlet oxygen atom $O(^1D)$ reactions with C_2H_2 and the kinetics of subsequent reactions via selective and time resolved detection of HO_2 and OH radicals by using FRS in a balanced detection scheme[28] to effectively cancel common-mode spectral interference.

2. Experimental Section

In this study, we developed a new photolysis flow reactor to study the reactions between $O(^1D)$ and C_2H_2 by combining mid-infrared FRS with direct UV-IR TDLAS. (Figure 1).

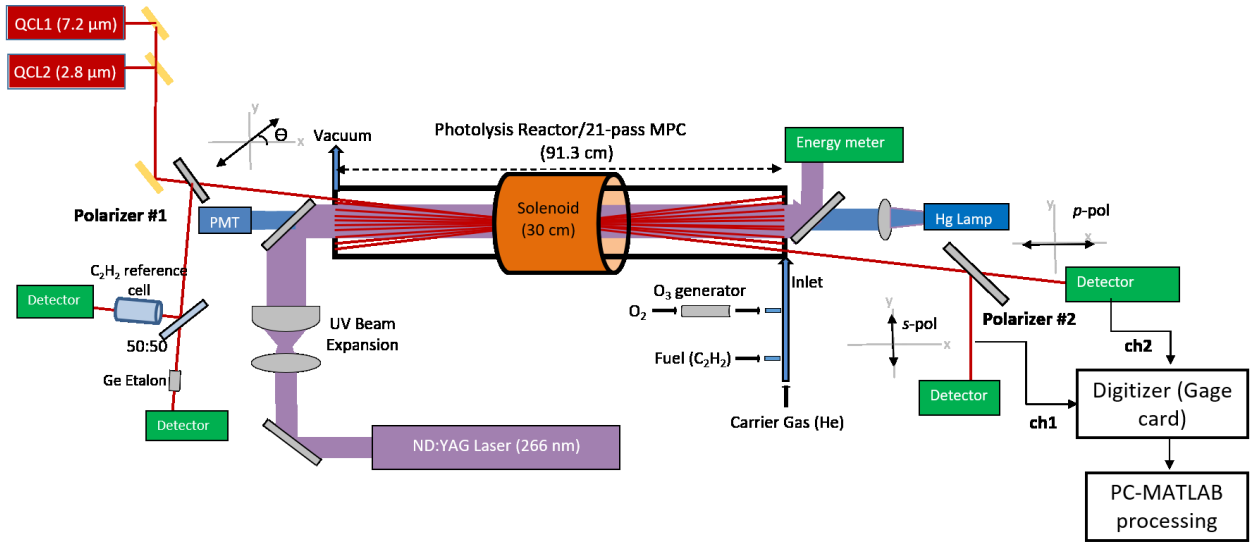

Figure 1. Experimental setup schematic.

The reactor is made of quartz tubing with an inner diameter of 56 mm. A pair of spherical mirrors with 250 mm focal length are installed at the both ends of the reactor 913 mm apart to form the multi-pass configuration (MPC) for the QCLs (7.2 µm, Thorlabs and 2.8 µm, Nanoplus) beams. A protective gold coating extends 8 mm from the edge of the mirror, leaving a 20º section transparent for the IR probe beam to couple into the photolysis cell. The uncoated central part of the spherical mirrors, 40 mm in diameter, allows for the UV photolysis beam to pass through the cell. Two dichroic mirrors (OMEGA OPTICAL) mounted at 45º are placed at the entrance and exit of the flow reactor to allow coupling of both UV photolysis beam and O_3 monitor beam (HG-1 Ocean Optics) in a single-pass configuration. A beam expander consisting of a UV coated plano-concave lens (f = -30 mm) and a UV coated plano-convex lens (f = 200 mm) were used to improve the homogeneity of the photolysis beam. The measured UV beam profile indicates that the uniformity across the reactor cross-section is ± 8.4 % from the mean value.

Kinetic model is developed based on HP-Mech (C0 – C2)[29-30] with electronically excited species sub-mechanism. The updated HP-Mech was attached in the supplementary material, in which the

$O(^1D)$ and electronically excited oxygen molecule $O_2(^1\Sigma)$ quenching reactions and reactions with O_3, H_2, H_2O_2, CH_4, H_2O, CH_2O, H, H_2O, CH_3 and C_2H_2 were considered. The half-life of diffusion time for major radicals and atoms out of photolysis beam (50 ms – 100 ms) are more than five times larger than HO_2 radicals decay time (ca. 10 ms) and almost two orders longer compared with OH radical decay time (ca. 1 ms). Thus, the photolysis reactor could be simulated by using closed homogeneous batch reactor (0-D) in Chemkin.

The absolute concentration of $O(^1D)$ was quantified by measuring the photon flux inside the reactor[1] using the absorption cross-section and the photolysis reaction pathway of O_3 at 266 nm at 60 Torr and 296 K. Ozone concentration is measured by a photomultiplier tube (Hamamatsu R7154) with amplifier (Hamamatsu C6271) using DAS signals from the monochromator (Acton 2500i). To avoid interferences from residual photolysis light or fluorescence from any surface, a 254 nm mercury line filter (Semrock) is installed before the monochromator. The major source of uncertainty in determining absolute concentration of $O(^1D)$ is quantifying the photolysis laser intensity inside the reactor. Therefore, we used *in-situ* laser light actinometry based on ozone depletion, which is relatively stable at these conditions, with detailed characterization of the cross-section at the monitoring wavelength of 253.65 nm (Mercury line).[31] Ozone depletion in this measurement occurs in two stages, as seen in Figure 2. The first stage is direct photolysis depletion: $O_3 + h\nu \rightarrow O(^1D) + O_2$ and $O_3 + h\nu \rightarrow O(^3P) + O_2$. The second stage is chemical reaction consumption: a decay in ozone concentration due to excited oxygen atoms $O(^1D)$ and excited oxygen molecules $O_2(^1\Sigma)$ interaction with O_3. The main reactions for stage 2 are: $O(^1D) + O_2 \rightarrow O(^3P) + O_2(^1\Sigma)$, $O_2(^1\Sigma) + O_3 \rightarrow O(^3P) + 2O_2$ and $O(^1D) + O_3 \rightarrow 2O_2$. The photon fluence F (photons cm^{-2}) can be calculated based on the absorbance (Abs):

$$F = \frac{Abs}{\sigma O3,253.65 * L * [O3] * \sigma O3,266} \quad (5)$$

where the ozone absorption cross-section at 253.65 nm and 266 nm are

$$\sigma_{O3,253.65} = (1.136 \pm 0.012) \times 10^{-17} \text{ cm}^2 \text{ molecule}^{-1} \quad (6)$$

$$\sigma_{O3,266} = (9.04 \pm 0.64) \times 10^{-18} \text{ cm}^2 \text{ molecule}^{-1} \quad (7)$$

L = 913 mm is the length of the reactor, and $[O_3]$ is the concentration. Actinometry measurements were performed before spectroscopy experiments to provide the absolute concentration of $O(^1D)$ atoms.

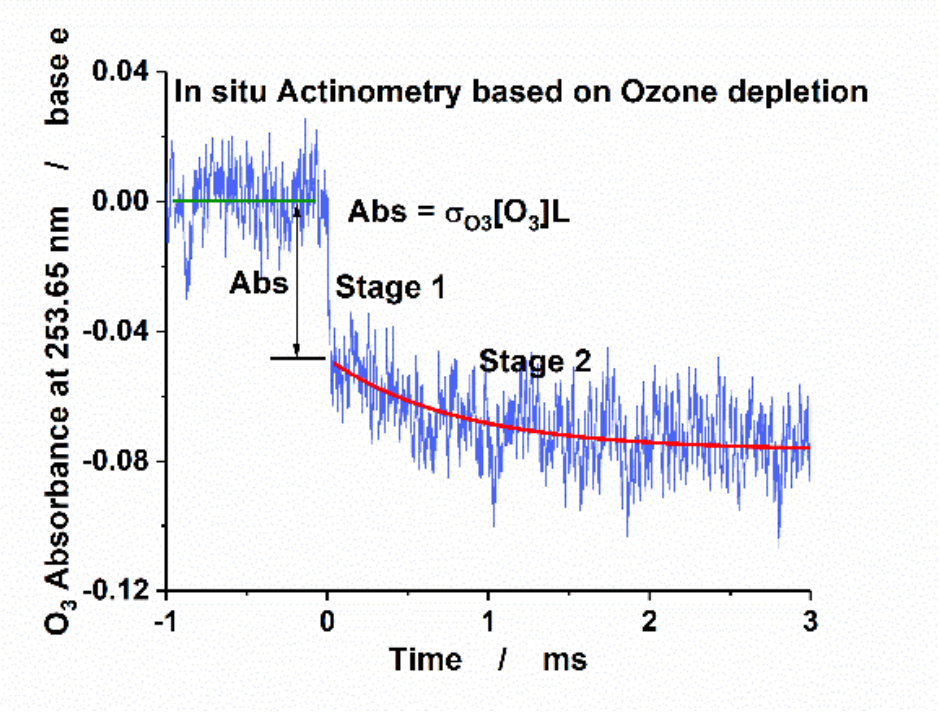

Figure 1. *In-situ* actinometry based on ozone depletion. Ozone is detected at the monitoring wavelength of 253.65 nm (Mercury line). Ozone depletion in this measurement occurs in two stages. The first stage is direct photolysis depletion: $O_3 + h\nu \rightarrow O(^1D) + O_2$ and $O_3 + h\nu \rightarrow O(^3P) + O_2$. The second stage is chemical reaction consumption: a decay in ozone concentration due to excited oxygen atoms $O(^1D)$ and excited

oxygen molecules $O_2(^1\Sigma)$ interaction with O_3. Green line is linear fitting before UV photolysis. Red line is fitted by HP-Mech which photon fluence is fitting parameter.

In the presence of a paramagnetic species such as HO_2, magnetically induced circular birefringence (MCB) causes rotation of the polarization plane of linearly polarized light, which leads to the FRS signal. As Figure 1 shows, a solenoid is used to generate an axial magnetic field (370 Gauss) along the direction of laser propagation within the flow reactor. A pair of wire-grid polarizers are used: one defines the incident linear polarization, and the second serves as an analyzer to convert laser polarization rotation into intensity changes that can be detected using photodetectors. In this case, the analyzer (Polarizer #2) axis is rotated at an angle of 45º with respect to the initial polarizer (Polarizer #1), hence the exit beam is split into the *s* and *p* orthogonal polarizations in the transmitted and reflected beam. In this balanced detection configuration, the FRS signal is obtained from the differential measurement between the *s* and *p* polarizations while other signals, including non-paramagnetic absorptions, appear as common mode signal.[32-33]

The advantage of this detection scheme is demonstrated in Figure 3, where we compare the TDLAS absorption spectra and FRS spectra observed at 7.2 μm under the same experimental conditions. Figure 3(a) shows the saw-tooth laser frequency scanning across the HO_2 transitions at a rate of 10 kHz, leading to an acquisition time of 100 μs for each spectrum. A total of 5 consecutive spectra are shown here, with ozone photolysis initiated after the second ramp. The TDLAS spectra is shown in panel (b), where 4 C_2H_2 lines are clearly visible and labeled in the figure. After the photolysis reactions, the HO_2 absorption signal appears near a dominant C_2H_2 transition as also labeled in panel (b). At 60 Torr, the HO_2 signal is still distinguishable from C_2H_2 but is already affected by the C_2H_2 lines. This spectral interference is effectively suppressed in the

FRS signal as shown in panel (c), where HO_2 formation is clearly visible after photolysis starts. HO_2 concentration is determined by least mean square fitting to the FRS spectrum using HITRAN line parameters. Due to the use of helium as the bath gas, collisional line-broadening parameters deviate from the air-broadening coefficients provided by HITRAN. Based on a well-calibrated frequency axis using a Germanium etalon, the actual broadening coefficient is determined during the nonlinear fitting procedure based on the best fit to the measured spectrum.

It should be noted that at higher pressures, collisional line broadening will result in more severe overlap between this interference and the HO_2 absorption signal, therefore the immunity to spectral interference from non-paramagnetic species makes FRS a uniquely suitable technique for *in-situ* measurements of radical species over a wide range of experimental conditions (e.g. with varying pressure and different fuels). In addition, given the clean signal spectrum achievable using FRS, spectral line-fitting is not required to isolate the HO_2 signal, which would be critical in the case shown in panel (b). Hence line-locked harmonic detection can be performed using fast laser wavelength modulation (e.g. at 100 kHz) to further improve sensitivity and time resolution of FRS detection.

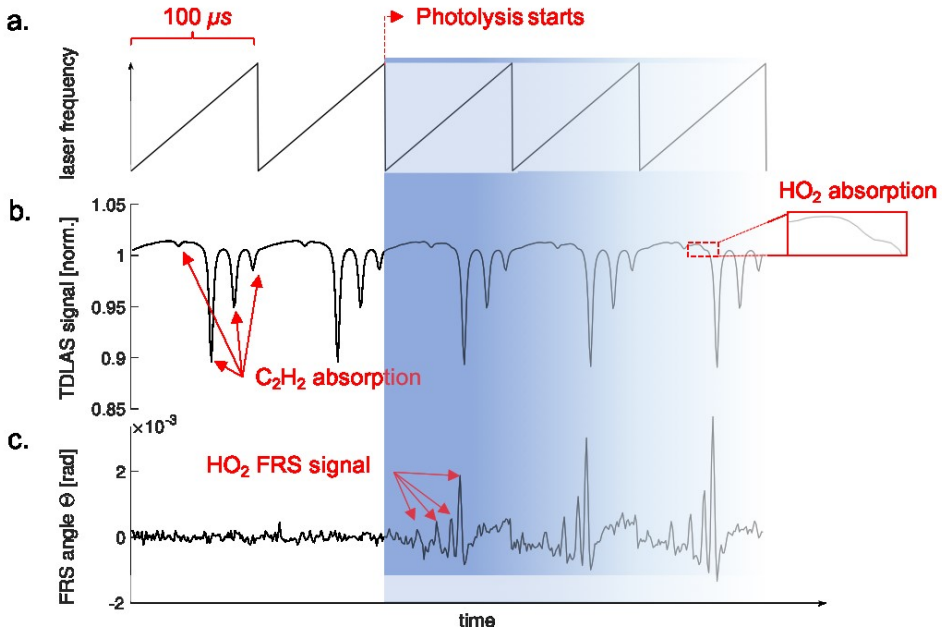

Figure 3. Illustration of spectral interference removal using FRS. (a) Continuous linear laser frequency scanning at a rate of 10 kHz from 1396.8 cm^{-1} to 1396.95 cm^{-1}. A total of 5 consecutive spectra are recorded with UV photolysis initiated after the second ramp. (b) TDLAS spectra containing both C_2H_2 and HO_2 absorption signal with prominent C_2H_2 features in the same spectral region. A zoomed view of HO_2 absorption is shown to emphasize the magnitude of spectral interference compared to the HO_2 signal using TDLAS. c) FRS spectra measured in the same experimental condition as (b). Note the absence of non-paramagnetic C_2H_2 absorptions.

In addition to HO_2, time-resolved concentration measurements of OH and H_2O are also required for modeling the chemical reaction pathways. In the current setup, another QCL at 2.8 μm is used for measuring OH and H_2O generated during the reactions following ozone photolysis. Since negligible spectral interference between OH and nearby water lines is observed at the current pressure conditions (60 Torr), TDLAS is used for detecting both OH and H_2O. QCL laser frequency fluctuations up to 0.003 nm is observed during the OH measurements. Since this

fluctuation is 4 times smaller than the full width at half maximum (FWHM) of OH absorption profiles at 60 Torr and 296 K according to HITRAN simulations, insignificant influence to concentration retrieval is assumed. The absorption cross-section of the OH radical at 3568.52 cm^{-1} is calibrated using well studied chemical reactions $O_3 + h\nu \rightarrow O(^1D) + O_2$ and $O(^1D) + H_2O \rightarrow 2\ OH$. The obtained absorption cross section is:

$$\sigma_{OH,3568.52cm\text{-}1} = (3.1 + 0.5) \times 10^{-18}\ cm^2\ molecule^{-1} \quad (8)$$

It should be noted, however, that with minor modifications to the current system, OH detection using FRS can be implemented to allow measurements at higher reactor pressures where interference becomes significant. The absorption cross section of H_2O at 3568.29 cm^{-1} is:

$$\sigma_{H2O,3568.29cm\text{-}1} = 2.45 \times 10^{-19}\ cm^2\ molecule^{-1} \quad (9)$$

at 60 Torr, which is taken from the HITRAN database.[34]

3. Results and discussion

In Figure 4(a), the OH radical absorption was measured at 3568.52 cm^{-1} at 60 Torr and ambient temperature. A large discrepancy has been found when comparing the experimental data with the original HP-Mech mechanism. However, by including the reaction $C_2H_2 + OH + M$ (R2), which is a dominant channel in low temperature fuel reaction, good agreement between the experimental results and model prediction is observed.

It is interesting to note in Figure 4(a) that the peak of OH production is observed 200 μs after photolysis, which indicates that the channel $O(^1D) + C_2H_2 \rightarrow C_2H + OH$ (R1d) via H abstraction reaction channel channel forming OH can be neglected because these channels would result in much faster OH rise (ca. 1 μs). This result is different from the previous studies of $O(^1D)$ reaction with saturated hydrocarbons,[10, 15, 35] suggesting the uniqueness of $O(^1D)$ reaction with unsaturated

hydrocarbons. According to the path flux analysis based on the reaction mechanism, channels 1b and 1c, as mentioned in the introduction, have similar sensitivities of OH formation, while channel 1a also displays significant sensitivity but in the opposite direction, to consume OH. As a result, combining a rough adjustment of the ratio of $k_{1a}/(k_{1b}+k_{1c})$ and a fine adjustment of the ratio of k_{1b}/k_{1c}, the agreement between simulation and experimental data was greatly improved. The derived branching ratios of channels 1a, 1b and 1c are 56%, 22% and 22%, respectively.

Figure 4(b) shows the H_2O formation measured using TDLAS at 3568.29 cm^{-1} to validate the updated kinetic mechanism (HP-Mech) which including the branching ratios of $O(^1D)$ reaction with C_2H_2 and key elementary reactions shown in table 1. The simulation agrees well with experimental measurement, especially during the initial H_2O rise but slightly overpredicts the H_2O concentration at around 1 ms. Signal fluctuation is observed from the minor drifting of the laser wavelength which can not substracted by the background measurements.

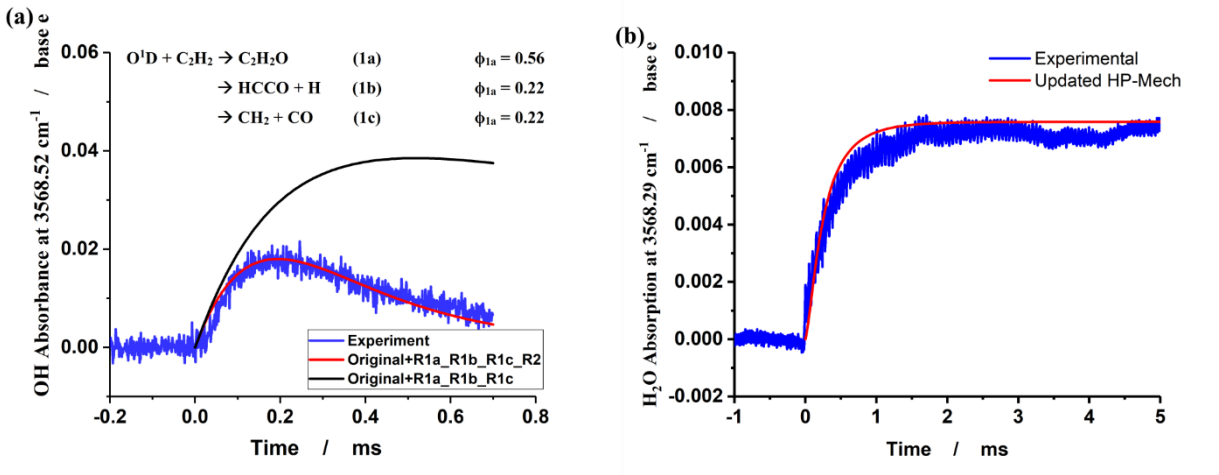

Figure 4. Comparison of the experimental data and simulation based on updated HP-Mech. (a) The time-resolved measurement of OH radicals. The critical reaction C_2H_2 + OH + M (R2) was missing in the HP-Mech which is the domain pathway for OH consumption. In this experimental condition, the recommendation channel is dominant (branching ratio φ_{1a} = 56%), while channel $O(^1D)$ +

C_2H_2 → C_2H + OH (R1d) can be neglected. (b) The time-resolved measurement of H_2O was measured at 3568.29 cm^{-1} wavenumber. There is good agreement between the experimental measurement and theoretical simulation based on the updated HP-Mech.

The path flux analysis indicated that the original mechanism constructed using HP-Mech and ozone measurements with additional reactions involving $O(^1D)$ has little sensitivity to the production of HO_2, suggesting the absence of some critical reaction channels for HO_2. Comparing with vinyl radicals, C_2H_3, 2-hydroxyvinyl radicals, C_2H_2OH has similar structure which is missing in most combustion models. According to the reaction between C_2H_3 and O_2, the reaction between 2-hydroxyvinyl radicals, C_2H_2OH, and O_2, might produce HCO and HCOOH:

$$C_2H_2OH + O_2 \rightarrow HCO + HCOOH \quad R3 \qquad (10)$$

In fact, Figure. 5 shows dramatically improved agreement between HO_2 measurements and the model prediction after including reaction R3. The reaction R3 is directly sensitive towards the HCO radical production, which is one of the most important intermediates in HO_2 formation. Using the HO_2 temporal profile, the corresponding rate constant of R3 was determined to be k_{R3} = $(5 \pm 2.5) \times 10^{11}$ cm^3 $mole^{-1}$ s^{-1} at 296 K and 60 Torr.

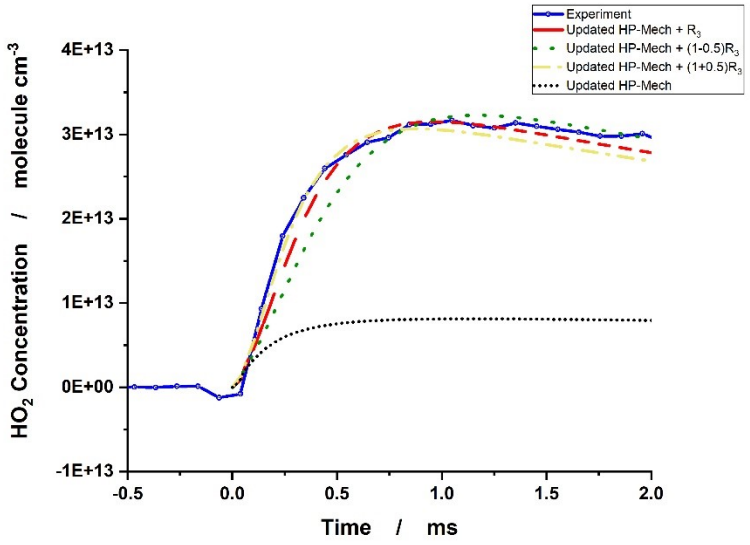

Figure 5. The temporal profile of HO_2 concentration with a gas mixture of $C_2H_2/O_2/O_3$/He. A key elementary reaction R3 ($C_2H_2OH+O_2$) dominates the HO_2 formation. The rate constant is determined by comparing the experimental profile with the updated HP-Mech simulation.

The branching ratios and rate constants of key reactions examined in this study are summarized in Table 1.

Table 1: Rate constants of key elementary reactions used in the simulation. The detailed HP-Mech can be found in the supporting materials. Units are in moles, cubic centimeters, seconds and cal/mole.

Number	*Reaction*	*A*	*n*	*Ea*	*Comments*
R1a	$O(^1D)+C_2H_2 \rightarrow HCCOH$	1.0e14	0	0	56% of k_{1total}
R1b	$O(^1D)+C_2H_2 \rightarrow HCCO+H$	4.0e13	0	0	22% of k_{1total}
R1c	$O(^1D)+C_2H_2 \rightarrow CH_2+CO$	4.0e13	0	0	22% of k_{1total}
R2	$C_2H_2+OH+M \rightarrow C_2H_2OH+M$	2.28e19	0	1071	Ref.[36-37]
R3	$C_2H_2OH+O_2 \rightarrow HCO+HCOOH$	5e11	0	0	This study

4. Conclusion

In conclusion, the kinetics of $O(^1D)$ reactions with C_2H_2 are studied through quantitative time-resolved measurements of HO_2, OH, H_2O, and $O(^1D)$ in a newly developed photolysis flow reactor. In particular, selective and time-resolved detection of HO_2 was successfully demonstrated through use of Faraday rotation spectroscopy by the suppression of spectral interference from non-paramagnetic hydrocarbon absorption via balanced detection. The branching ratios of $O(^1D)$ reactions with C_2H_2 as well as its subsequent reaction kinetics are quantified. It was found that differing from $O(^1D)$ reaction with saturated hydrocarbons, the OH formation channel via direct H abstraction is negligible in $O(^1D)$ reactions with unsaturated C_2H_2. This finding suggests the

uniqueness of $O(^1D)$ reaction with unsaturated hydrocarbons. Moreover, the retrieved HO_2 temporal profile allows for identification and determination of the rate constant of a missing reaction channel for HO_2 production involving C_2H_2OH with O_2. Furthermore, with the time-dependent OH measurement, another missing reaction channel via $C_2H_2+OH+M \rightarrow C_2H_2OH+M$ was also identified.

With the adoption of these reaction channels and the measured reaction rates and branching ratios, an updated kinetic model for $O(^1D)$ reactions with $O(^1D)$ based on HP-Mech is developed. The updated model significantly improved the prediction of experimental results of OH, HO_2, and H_2O. The results also demonstrate that the new experimental apparatus combing TDLAS with FRS in the photolysis reactor has the potential for sensitive measurements of many species. (e.g. OH, HO_2, H_2O, CH_2O, C_2H_2, and O_3) for the study more complicated chemical kinetics and dynamics involving $O(^1D)$ reaction with large unsaturated hydrocarbons and oxygenated fuels. Furthermore, understanding of $O(^1D)$ reactions with fuels provides a key sub-mechanism of reaction kinetics for combustion, plasma chemistry, materials synthesis, and atmospheric chemistry.

Acknowledgement

This project is supported by the NSF grants CBET 1903362 and 1507358 , DOE grant DE-SC0020233 of Plasma Science Cen- ter, Princeton SEAS innovation grant, ACEE center grant, and Exxon Mobile research grant.

Supporting Information:

Experimental conditions; Updated kinetic model based on the modified HP-Mech.

AUTHOR INFORMATION

Corresponding Author

*Email: chaoy@princeton.edu

ORCID

Chao Yan: 0000-0002-2415-6080

Present Address

Department of Mechanical & Aerospace Engineering Department, Princeton University, Princeton, NJ, 08540, United States.

Notes

The authors declare no competing financial interests.

Acknowledgement: This project is supported by the NSF CBET-1507358, Princeton SEAS innovation grant, ACEE center grant, and Exxon Mobile research grant.

Table of Contents Graphic:

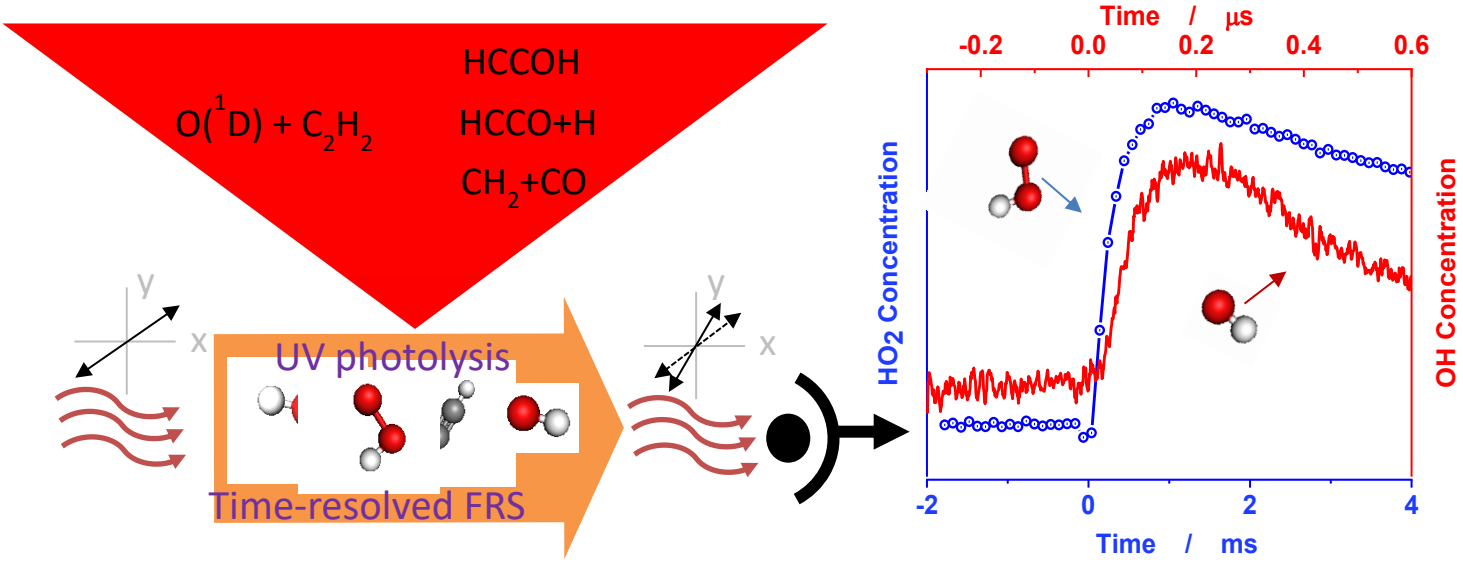

Reference

1. Dunlea, E. J.; Ravishankara, A. R., Kinetic studies of the reactions of O(1D) with several atmospheric molecules. *Physical Chemistry Chemical Physics* **2004,** *6* (9), 2152-2161.
2. Vranckx, S.; Peeters, J.; Carl, S., Kinetics of O(1D) + H2O and O(1D) + H2: absolute rate coefficients and O(3P) yields between 227 and 453 K. *Physical Chemistry Chemical Physics* **2010,** *12* (32), 9213-9221.
3. Ju, Y.; Sun, W., Plasma assisted combustion: Dynamics and chemistry. *Progress in Energy and Combustion Science* **2015,** *48* (Supplement C), 21-83.
4. Suo, Y.; Sharath, N.; Wenting, S.; Vigor, Y., Multiscale modeling and general theory of non-equilibrium plasma-assisted ignition and combustion. *Journal of Physics D: Applied Physics* **2017,** *50* (43), 433001.
5. Yang, S.; Gao, X.; Yang, V.; Sun, W.; Nagaraja, S.; Lefkowitz, J. K.; Ju, Y., Nanosecond Pulsed Plasma Activated C2H4/O2/Ar Mixtures in a Flow Reactor. *Journal of Propulsion and Power* **2016,** *32* (5), 1240-1252.
6. Welz, O.; Klippenstein, S. J.; Harding, L. B.; Taatjes, C. A.; Zádor, J., Unconventional Peroxy Chemistry in Alcohol Oxidation: The Water Elimination Pathway. *The Journal of Physical Chemistry Letters* **2013,** *4* (3), 350-354.
7. Skodje, R. T.; Tomlin, A. S.; Klippenstein, S. J.; Harding, L. B.; Davis, M. J., Theoretical Validation of Chemical Kinetic Mechanisms: Combustion of Methanol. *The Journal of Physical Chemistry A* **2010,** *114* (32), 8286-8301.
8. Prather, M. J., Time Scales in Atmospheric Chemistry: Coupled Perturbations to N₂O, NO_y, and O₃. *Science* **1998,** *279* (5355), 1339-1341.

9. Gligorovski, S.; Strekowski, R.; Barbati, S.; Vione, D., Environmental Implications of Hydroxyl Radicals (•OH). *Chemical Reviews* **2015,** *115* (24), 13051-13092.
10. Lin, C. L.; DeMore, W. B., Reactions of atomic oxygen (1D) with methane and ethane. *The Journal of Physical Chemistry* **1973,** *77* (7), 863-869.
11. Luntz, A. C., Chemical dynamics of the reactions of O(1D2) with saturated hydrocarbons. *The Journal of Chemical Physics* **1980,** *73* (3), 1143-1152.
12. Yamazaki, H.; Cvetanović, R. J., Collisional Deactivation of the Excited Singlet Oxygen Atoms and Their Insertion into the CH Bonds of Propane. *The Journal of Chemical Physics* **1964,** *41* (12), 3703-3710.
13. Yang, X., Multiple channel dynamics in the O(1D) reaction with alkanes. *Physical Chemistry Chemical Physics* **2006,** *8* (2), 205-215.
14. Yu, H.-G.; Muckerman, J. T., MRCI Calculations of the Lowest Potential Energy Surface for CH3OH and Direct ab Initio Dynamics Simulations of the O(1D) + CH4 Reaction. *The Journal of Physical Chemistry A* **2004,** *108* (41), 8615-8623.
15. Wada, S.-i.; Obi, K., Photochemical Reaction Dynamics of O(1D) with Saturated Hydrocarbons, CH4, C2H6, and C3H8, under Bulk Conditions and in van der Waals Complexes. *The Journal of Physical Chemistry A* **1998,** *102* (20), 3481-3491.
16. Carl, S. A., A highly sensitive method for time-resolved detection of O(1D) applied to precise determination of absolute O(1D) reaction rate constants and O(3P) yields. *Physical Chemistry Chemical Physics* **2005,** *7* (24), 4051-4053.
17. Girard, Y.; Chaquin, P., Addition Reactions of 1D and 3P Atomic Oxygen with Acetylene. Potential Energy Surfaces and Stability of the Primary Products. Is Oxirene Only a Triplet Molecule? A Theoretical Study. *The Journal of Physical Chemistry A* **2003,** *107* (48), 10462-10470.
18. Chen, M.-W.; Rotavera, B.; Chao, W.; Zádor, J.; Taatjes, C. A., Direct measurement of ˙OH and HO2˙ formation in ˙R + O2 reactions of cyclohexane and tetrahydropyran. *Physical Chemistry Chemical Physics* **2018,** *20* (16), 10815-10825.
19. DeSain, J. D.; Ho, A. D.; Taatjes, C. A., High-resolution diode laser absorption spectroscopy of the O – H stretch overtone band (2,0,0)←(0,0,0) of the HO2 radical. *Journal of Molecular Spectroscopy* **2003,** *219* (1), 163-169.
20. Wallington, T. J.; Dagaut, P.; Kurylo, M. J., UV absorption cross sections and reaction kinetics and mechanisms for peroxy radicals in the gas phase. *Chemical Reviews* **1992,** *92* (4), 667-710.
21. Heard, D. E.; Pilling, M. J., Measurement of OH and HO2 in the Troposphere. *Chemical Reviews* **2003,** *103* (12), 5163-5198.
22. Clemitshaw, K., A Review of Instrumentation and Measurement Techniques for Ground-Based and Airborne Field Studies of Gas-Phase Tropospheric Chemistry. *Critical Reviews in Environmental Science and Technology* **2004,** *34* (1), 1-108.
23. Thiébaud, J.; Fittschen, C., Near infrared cw-CRDS coupled to laser photolysis: Spectroscopy and kinetics of the HO2 radical. *Applied Physics B* **2006,** *85* (2), 383-389.
24. DeSain, J. D.; Klippenstein, S. J.; Miller, J. A.; Taatjes, C. A., Measurements, Theory, and Modeling of OH Formation in Ethyl + O2 and Propyl + O2 Reactions. *The Journal of Physical Chemistry A* **2004,** *108* (34), 7127-7128.
25. Nizkorodov, S. A.; Harper, W. W.; Blackmon, B. W.; Nesbitt, D. J., Temperature Dependent Kinetics of the OH/HO2/O3 Chain Reaction by Time-Resolved IR Laser Absorption Spectroscopy. *The Journal of Physical Chemistry A* **2000,** *104* (17), 3964-3973.

26. Yan, C.; Kocevska, S.; Krasnoperov, L. N., Kinetics of the Reaction of CH3O2 Radicals with OH Studied over the 292–526 K Temperature Range. *The Journal of Physical Chemistry A* **2016,** *120* (31), 6111-6121.
27. Brumfield, B.; Sun, W.; Ju, Y.; Wysocki, G., Direct In Situ Quantification of HO2 from a Flow Reactor. *The Journal of Physical Chemistry Letters* **2013,** *4* (6), 872-876.
28. Brumfield, B.; Wysocki, G., Faraday rotation spectroscopy based on permanent magnets for sensitive detection of oxygen at atmospheric conditions. *Opt. Express* **2012,** *20* (28), 29727-29742.
29. Shen, X.; Yang, X.; Santner, J.; Sun, J.; Ju, Y., Experimental and kinetic studies of acetylene flames at elevated pressures. *Proceedings of the Combustion Institute* **2015,** *35* (1), 721-728.
30. Zhao, H.; Yang, X.; Ju, Y., Kinetic studies of ozone assisted low temperature oxidation of dimethyl ether in a flow reactor using molecular-beam mass spectrometry. *Combustion and Flame* **2016,** *173*, 187-194.
31. Sander, S.; Golden, D.; Kurylo, M.; Moortgat, G.; Wine, P.; Ravishankara, A.; Kolb, C.; Molina, M.; Finlayson-Pitts, B.; Huie, R. *Chemical kinetics and photochemical data for use in atmospheric studies evaluation number 15*; Pasadena, CA: Jet Propulsion Laboratory, National Aeronautics and Space Administration, 2006: 2006.
32. Johansson, A. C.; Westberg, J.; Wysocki, G.; Foltynowicz, A., Optical frequency comb Faraday rotation spectroscopy. *Applied Physics B* **2018,** *124* (5), 79.
33. Westberg, J.; Wysocki, G., Cavity ring-down Faraday rotation spectroscopy for oxygen detection. *Applied Physics B* **2017,** *123* (5), 168.
34. Gordon, I. E.; Rothman, L. S.; Hill, C.; Kochanov, R. V.; Tan, Y.; Bernath, P. F.; Birk, M.; Boudon, V.; Campargue, A.; Chance, K. V.; Drouin, B. J.; Flaud, J. M.; Gamache, R. R.; Hodges, J. T.; Jacquemart, D.; Perevalov, V. I.; Perrin, A.; Shine, K. P.; Smith, M. A. H.; Tennyson, J.; Toon, G. C.; Tran, H.; Tyuterev, V. G.; Barbe, A.; Császár, A. G.; Devi, V. M.; Furtenbacher, T.; Harrison, J. J.; Hartmann, J. M.; Jolly, A.; Johnson, T. J.; Karman, T.; Kleiner, I.; Kyuberis, A. A.; Loos, J.; Lyulin, O. M.; Massie, S. T.; Mikhailenko, S. N.; Moazzen-Ahmadi, N.; Müller, H. S. P.; Naumenko, O. V.; Nikitin, A. V.; Polyansky, O. L.; Rey, M.; Rotger, M.; Sharpe, S. W.; Sung, K.; Starikova, E.; Tashkun, S. A.; Auwera, J. V.; Wagner, G.; Wilzewski, J.; Wcisło, P.; Yu, S.; Zak, E. J., The HITRAN2016 molecular spectroscopic database. *Journal of Quantitative Spectroscopy and Radiative Transfer* **2017,** *203*, 3-69.
35. Full characterization of OH product energetics in the reaction of O(1D2) with hydrocarbons. *The Journal of Chemical Physics* **1991,** *95* (11), 8166-8177.
36. McKee, K. W.; Blitz, M. A.; Cleary, P. A.; Glowacki, D. R.; Pilling, M. J.; Seakins, P. W.; Wang, L., Experimental and Master Equation Study of the Kinetics of OH + C2H2: Temperature Dependence of the Limiting High Pressure and Pressure Dependent Rate Coefficients. *The Journal of Physical Chemistry A* **2007,** *111* (19), 4043-4055.
37. Senosiain, J. P.; Klippenstein, S. J.; Miller, J. A., The Reaction of Acetylene with Hydroxyl Radicals. *The Journal of Physical Chemistry A* **2005,** *109* (27), 6045-6055.